Check for updates

Multilayered MoAlB@MBene structures using mild microwave-assisted etching and their optical properties†

Madhurya Chandel, [iD] *[a] Muhammad Abiyyu Kenichi Purbayanto, [iD] [a]
Dominik Kowal,[b] Dorota Moszczyńska,[c] Anna Wójcik,[d]
Muhammad Danang Birowosuto, [iD] [b] Michael Naguib [iD] [e] and
Agnieszka Maria Jastrzębska*[a]

MBenes, a novel class of transition metal borides, represent an exciting advancement in two-dimensional (2D) materials. This study introduces a novel and mild microwave-assisted hydrothermal method. A multi-layered (ML) MoAlB@MBene structure is achieved when a mixture of hydrochloric acid (HCl) and hydrogen peroxide (H_2O_2) is used in combination with acid (0.1 M HCl) or base (0.1 M NaOH) pre-treatment. This method differs from reported etching techniques, which require long reaction times and highly concentrated acids (or bases). Also, they demonstrated that instead of selectively etching, the MAB phases dissolve, incompletely etch, or even oxidize. Achieving a multilayer structure within 4 hours was previously challenging. The current process allows for ML MBene formation and controlled oxidation in 4 hours. This leads to a distinct bandgap opening in ML MoAlB@MBene, with energy levels of 3.54, 3.58, 3.65, and 3.88 eV. The study also explores the optical absorption characteristics and time-resolved photoluminescence (TRPL) behavior of ML MoAlB@MBene. This demonstrates its tunable optical properties and significant potential for applications in high-performance light-emitting diodes, photovoltaics, photocatalysts, laser diodes, and more.

New concepts

While MXenes have been extensively studied, MBenes remain largely unexplored. This study uses microwave-assisted hydrothermal techniques to introduce a new, efficient, and mild method for etching aluminum (Al) from the MoAlB MAB phase. Fully etching Al from MoAlB is challenging due to its dual-layer Al structure and the serpentine chain of boron atoms. The fundamental optical properties of these MBenes have not been thoroughly explored experimentally. Our innovative approach uses pre-treatments with acid (HCl) or base (NaOH) before hydrothermal, achieving better etching than previously reported methods requiring highly concentrated chemicals and longer durations. We systematically examine the impact of these pre-treatments, the effectiveness of microwave-assisted etching, and the resulting optical properties of MoAlB-based MBenes. Variations in the band gap and optical absorption are linked to different etching techniques, functionalization of etched MoAlB, and formation of metal oxides (MoO_3 or Mo_2O_5) on its surface. These findings highlight the potential of MBenes for use in optical devices such as photodiodes and LEDs. Our work calls for further research into efficient etching and delamination methods to explore MBene applications in optoelectronics.

1. Introduction

The development of graphene has opened the door to other two-dimensional (2D) materials such as MXenes, transition metal dichalcogenides (TMDs), phosphorene, g-C_3N_4, *etc.* In this 2D nanomaterials family, MBenes are relatively new and intriguing members.[1–3] Theoretical research shows that MBenes could be obtained from their respective MAB phases, called layered ternary transition metal borides, as first reported in 1942 by Halla and Thury.[4] They are composed of face-sharing BM_6 trigonal prisms interleaved with bilayers of Al atoms.[1]

MAB phases show two typical structural variants such as the MAlB type (space group *Cmcm*) and M_2AlB_2 type (space group *Cmmm*) and the rarer $M_3Al_2B_2$, M_3AlB_4 and M_4AlB_6 types. In addition, the MAlB, M_2AlB_2, and $M_3Al_2B_2$ forms contain isolated serpentine chains of boron atoms, while the M_3AlB_4 and M_4AlB_6 contain double and triple chains of boron atoms, respectively.[1,5]

In 1966, Jeitschko confirmed the crystal structure of MoAlB to be orthorhombic, with the space group *Cmcm*.[6] MoAlB is orthorhombic, with MoB bilayers that alternate with two Al

[a] *Warsaw University of Technology, Faculty of Mechatronics, św. Andrzeja Boboli 8, 02-525 Warsaw, Poland. E-mail: madhurya.chandel@pw.edu.pl, agnieszka.jastrzebska@pw.edu.pl*

[b] *Łukasiewicz Research Network-PORT Polish Center for Technology Development, Stabłowicka 147, 54-066, Wrocław, Poland*

[c] *Warsaw University of Technology, Faculty of Materials Science and Engineering, Wołoska 141, 02-507, Poland*

[d] *Polish Academy of Sciences, Institute of Metallurgy and Materials Science, W. Reymonta 25, 30-059 Cracow, Poland*

[e] *Tulane University, Department of Physics and Engineering Physics, New Orleans, LA 70118, USA*

† Electronic supplementary information (ESI) available. See DOI: https://doi.org/10.1039/d4mh01500b

layers, resulting in a layered crystal structure. MoAlB is an attractive target for creating 2D metal boride through the exfoliation of MoAlB using chemical etching.[7] Although hexagonal MAB phases are prone to etching into single-layered MBenes they are unstable, whereas orthorhombic phases could be used to obtain other structures. However, preliminary attempts have shown that it is challenging to completely etch out Al from an orthorhombic MAB phase (MoAlB).[7–11]

Alameda et al. observed that Al layers are partially etched out from MoAlB powder by a 10% NaOH solution and yield MoAlB slabs with 50–300 nm thickness and 10–100 nm spacing between layers. The X-ray diffraction patterns showed that the MoAlB retained its crystal structure after the etching treatment.[7] When hydrofluoric (HF) acid was used, it resulted in the absence of etching and the formation of a fluorine-containing coating.[7]

In another attempt, Alameda et al. achieved a partial deintercalation of Al from MoAlB single crystals using 10% NaOH (aqueous solution) and a solution of 2 M LiF (lithium fluoride) in 6 M HCl (hydrochloric acid) at room temperature for 2 and 24 h, respectively.[10] They observed that NaOH etching creates about 10 nm wide cavities at the crystal surface, distributed periodically every 100–200 nm. In the case of LiF/HCl, in addition to Al deintercalation, extensive corrosion of the boride layer was observed along with etched "branches", which propagated in [010], corroding through MoB layers to form a network of cavities.[7,10,12] Significant corrosion was observed when using the widely reported 40% HF procedure for MXene synthesis, and there was some evidence of Al layer removal in MoAlB.[7,10] Apart from etching, a layer of fluorine was formed on the whole surface of the MAB phase.[7,10–12]

Recently, two additional attempts have been made. First, Majed et al. reported using 10% NaOH for 24 and 96 hours, resulting in a multilayer with porous morphologies and transforming MoAlB into Mo_2AlB_2.[9] In another attempt, Bury et al. used 9 M HCl and 0.3% H_2O_2 for 24, 48, and 72 hours to etch out Al. The colloidal solution gradually changed from dark grey to green and greenish-blue throughout the etching process, then back to light grey. After 48 hours, they observed delaminated 2D MBene flakes with smooth, non-oxidized surfaces and edges.[13] However, after 72 hours, the flakes became irregularly defective and torn, showing surface oxidation, likely due to prolonged exposure to harsh chemicals.

Considering the available knowledge, we have developed a mild microwave-assisted hydrothermal route for the surface-oriented etching process of orthorhombic MoAlB. The surface of MoAlB acts as a precursor for etching out the Al layers in the vicinity of MoAlB grains. The final multilayered (ML) MoAlB@MBene structure is achieved when a mixture of hydrochloric acid (HCl) and hydrogen peroxide (H_2O_2) is used in combination with acid (0.1 M HCl) or base (0.1 M NaOH) pretreatment. In summary, the newly developed method allows for precise control over the Al etching and oxidation degree of MoAlB@MBene, leading to intriguing optical properties.

Recently, researchers have investigated the optical properties of MBenes in different phases other than MoAlB, such as $(Mo_{2/3}Y_{1/3})_2AlB_2$. For instance, Guo et al. fabricated $Mo_{4/3}B_{2-x}T_z$ MBene by selectively etching Al and Y using aqueous hydrofluoric acid (HF) and studied its nonlinear absorption and saturation intensities.[14] Similarly, Wang et al. examined $Mo_{4/3}B_2T_x$ MBene, which displays a surface termination-dependent electronic structure, carrier dynamics, and nonlinear optical response across a wide wavelength range (500–1550 nm).[15]

However, a lack of comprehensive understanding and control of the optical properties remains unclear. Additionally, optical properties vary depending on each phase and the synthesis method used. Considering the previous reports,[7,10,13,16] a successful and selective etching out of Al from the MAB phase could open up new research activities in the MBene field. Therefore, further exploration of the different synthesis methodologies and properties of MBenes is needed.

2. Methods

2.1. Etching the MAB phase (MoAlB)

Here, we report three different approaches for etching MoAlB using the microwave-assisted hydrothermal method. The details of the methods, including the MAB phase MoAlB synthesis, are discussed in the ESI.†

A two-step process for Al etching has been employed: (i) pretreatment, and (ii) mild microwave-assisted hydrothermal treatment. To investigate the impact of pre-treatment on etching, an additional experiment was conducted without any pretreatment, directly proceeding to the hydrothermal method. For the pre-treatment, 250 mg of MoAlB was stirred in 0.1 M HCl/NaOH for two hours, then washed with double distilled water until the pH reached 6. Then, in the second stage, the washed residue was transferred into 20 mL of 0.6 M HCl (in water) solution with constant stirring, followed by sonication for 2 min. After that, 250 µL of H_2O_2 (30% (v/v) in H_2O) solution was added dropwise, and the Teflon container was closed.

After fitting the reactor, the reaction started with a reaction time of 2 h at 150 °C, with 480 W microwave power. In the end, the precipitate was washed using centrifugation (3000 rpm for 4 min) until the reaction mixture's pH reached 6. Here, the precursor MoAlB phase is denoted as it is (MoAlB), synthesis without pre-treatment as MAB@MBene, pre-treated with 0.1 M NaOH as Base-MAB@MBene, and pre-treated with 0.1 M HCl as Acid-MAB@MBene, which is shown in Fig. 1. Therefore, this work considers the following samples: MoAlB, MAB@MBene, Base-MAB@MBene, and Acid-MAB@MBene to differentiate structures prepared using different etching approaches.

2.2. Characterization

The morphology of MoAlB, MAB@MBene, Base-MAB@MBene, and Acid-MAB@MBene were studied using scanning electron microscopy (SEM Hitachi SU3500 Hitachi, Tokyo, Japan) and transmission electron microscopy (TEM, Philips CM 20, Amsterdam, Holland). The samples for SEM imaging were prepared on aluminum/silicon substrates. Energy-dispersive X-ray spectroscopy (EDS) was used to study the elemental
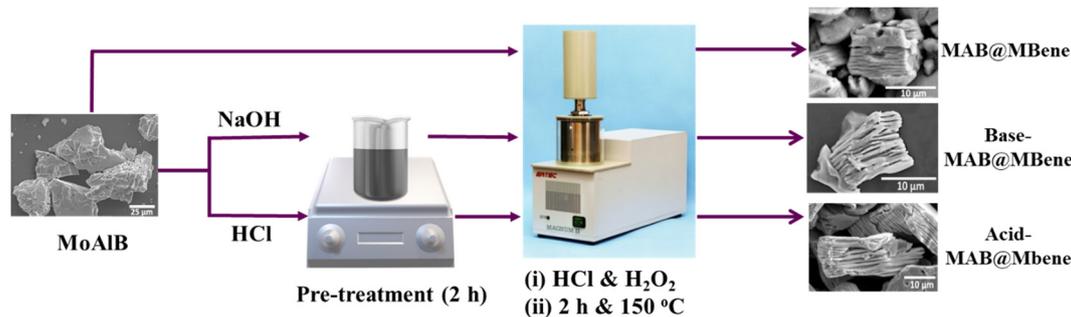
Fig. 1 The schematic diagram presents three protocols employed for surface-oriented aluminum etching (Al) from orthorhombic MoAlB. While one protocol considered direct MAB etching (MAB@MBene), the other two considered additional acid (Acid-MAB@MBene) or base (Base-MAB@MBene) pre-treatments.

composition of the samples. X-ray fluorescence (XRF) spectroscopy was used to check the Al (aluminum) and Mo (molybdenum) element percentages in the sample using a Pl-100 XRF laboratory spectrometer (POLON IZOT, Warsaw, Poland). X-ray diffraction (XRD) patterns were measured to evaluate the purity and crystal structure of the samples using a Bruker D8 Advance (Billerica, MA, USA).

The zeta potential was characterized by using a Zetasizer NANO ZS ZEN3500 analyzer (Malvern Instruments, Malvern, UK) equipped with a back-scattered light detector and operating at 173°. The results are presented based on an average of 10 repeated measurements. The surface functionalization and chemical composition were studied using attenuated total reflectance-Fourier transform infrared (ATR-FTIR) spectroscopy (Nicolet iS5, Thermo Electron, Waltham, MA, USA).

XPS was measured using a PHI 5000 Versa Probe (ULVAC-PHI) spectrometer equipped with monochromatic Kα radiation ($h\nu$ = 1486.6 eV). The X-ray source operates at a spot size of 100 μm, at 25 W and 15 kV. A hemispherical analyzer further acquired the spectra at a pass energy of 117.4 eV with an energy step size of 0.1 eV. The X-ray beam was aligned 45° to the sample surface in the measurement. Furthermore, the XPS fitting analysis was carried out using a Shirley background, in which all spectra were calibrated by C 1s adventitious carbon peaks (C–C) at 285 eV.

2.3. Optical measurements

The absorption spectra of the samples were studied using a double-beam scanning UV-vis spectroscope (Evolution 220, Thermo Scientific) equipped with an integrating sphere. The colloidal solution of the samples was prepared in water (4 mg mL^{-1}), and the absorbance was measured at a scanning speed of 200 nm min^{-1} for a 400–1000 nm wavelength range with an integration time of 0.3 s and a wavelength resolution of 1 nm. Water was used as a reference in the spectra acquisition. For powder samples, solid sample holders were used with quartz glass, and the data were taken using a diffuse reflectance (DRS) mode in the 400–1000 nm wavelength range with a scanning speed of 200 nm min^{-1}.

The optical constants (n and k) of the samples were acquired using spectroscopic ellipsometry (SE SENresearch 4.0, Sentech,

Germany) with an angle of measurement of 45°. To conduct the measurements, liquid dispersions of MBenes were first sonicated in solution for 2 hours and then drop cast onto a Si wafer. The multilayer nature of MBene crystallites, alongside challenges in achieving a uniform and continuous thin film of this material, presented obstacles in obtaining superior-quality data in reflection-based measurements.

Consequently, fitting the measurement results convincingly with oscillator-type models, such as the Tauc–Lorentz fit expected for bandgap materials, proved challenging. Instead, the data was fitted using a polynomial formula, as illustrated in Fig. S1 (ESI†). It should be noted that the presence of a significant air fraction within the multilayer material might also contribute to the observed experimental results being smaller than those predicted by previous theoretical studies on the MoAlB phase.[17] We used a thermoelectric-cooled AvaSpec-HERO spectrometer to collect the photoluminescence spectra. The samples were excited by a picosecond pulsed diode laser with a repetition rate of 30 kHz (Master Oscillator Fiber Amplifier, PicoQuant), operating at an excitation wavelength of 266 nm and a pulse width of 50 ps. The collection was done using a visible-near-infrared microscope objective (5×, NA = 0.15).

For time-resolved photoluminescence measurement, we analyzed the timing response using time-correlated single-photon counting electronics (Hydra-Harp400, PicoQuant, Germany). The TRPL decay curves were fitted with three exponential functions, and we determined the average lifetime from the decay time components and amplitudes of the fits.

3. Results and discussion

3.1. Etching methodologies

Due to hazardous environmental effects, researchers are moving toward soft synthesis approaches, in which hydrothermal/solvothermal and microwave-assisted methods play a significant role in controllable processes.[18] Combining hydrothermal and microwave heating reduces the reaction time while maintaining material quality. Microwave heating minimizes the reaction time from long hours in a traditional wet-chemical synthesis to several minutes.

In the hydrothermal method, high temperature and pressure help dissolve impurities that do not dissolve under typical conditions. It also helps to grow and prepare specific crystal structured and morphological material.[19] In addition, microwave heating helps to reduce the heat loss to almost zero. A Teflon container allows microwaves to pass through it, ensuring fast and even heating thanks to its low dielectric loss. Other synthesis methods can't replicate these unique benefits of microwave heating.[18,19]

Therefore, we assumed that by combining these two techniques we could enable multilayered (ML) structures of MBene from orthorhombic MoAlB MAB phases in a controllable manner. A schematic diagram of the microwave-assisted hydrothermal methods for etching Al from MoAlB is shown in Fig. 1.

Here, the starting MoAlB powder was divided into three parts. The first part underwent direct etching into MAB@MBene, while the other two underwent additional acid (Acid-MAB@MBene) or base (Base-MAB@MBene) pre-treatments. Pre-treatments with 0.1 M NaOH and 0.1 M HCl could initiate the etching before using a hydrothermal method to etch out the aluminum (Al) layer from the corresponding MAB phase.

3.2. Materials characterization

The MoAlB powder was soaked and stirred in 0.1 M NaOH and HCl for 2 hours to initiate the etching by opening up the edges. After pre-treatment, we observed some amount of Al etched and floating on the surface of the reaction mixture for both the NaOH and HCl pre-treatments, as presented in the ESI†

(inset Fig. S2a and b, respectively). The X-ray fluorescence (XRF) results (Fig. S2a and b, ESI†) confirmed the presence of Al in the supernatant. The peak intensity of Al in Acid-MAB@MBene supernatant is higher than in the Base MAB@MBene. This could further lead to better etching of MoAlB@MBene than MAB@MBene. Therefore, we could conclude that both 0.1 M NaOH and HCl could initiate the Al etching through basic Al reactivity with aqueous acid (HCl) and base (NaOH) according to reactions (1) and (2):[20]

$$2Al + 6HCl \rightarrow 2AlCl_3 + 3H_2 \quad (1)$$

$$2Al + 2NaOH + 2H_2O \rightarrow 2NaAl(OH)_4 + 3H_2 \quad (2)$$
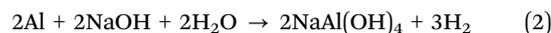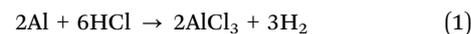
The microwave-assisted hydrothermal method based on an etching solution of 0.6 M HCl and H_2O_2 (from 30% water solution) was employed after the pre-treatments. Note that MoAlB was also etched without any pre-treatment for comparison purposes. After etching, we collected all three supernatants for MAB@MBene, Acid-MAB@MBene, and Base-MAB@MBene. We observed different colors, such as navy-blue supernatant for MAB@MBene (without any pre-treatment), as shown in the inset in Fig. 2a. A pale-yellow supernatant was obtained for Base-MAB@MBene (pre-treated with 0.1 M NaOH, inset in Fig. 2b) and Acid-MAB@MBene (pre-treated with 0.1 M HCl, inset in Fig. 2c).

The color of the supernatant changing from navy blue to pale yellow suggests the presence of Mo-oxidized species such as MoO_2OH (blue) and MoO_3 (pale yellow).[21] The presence of

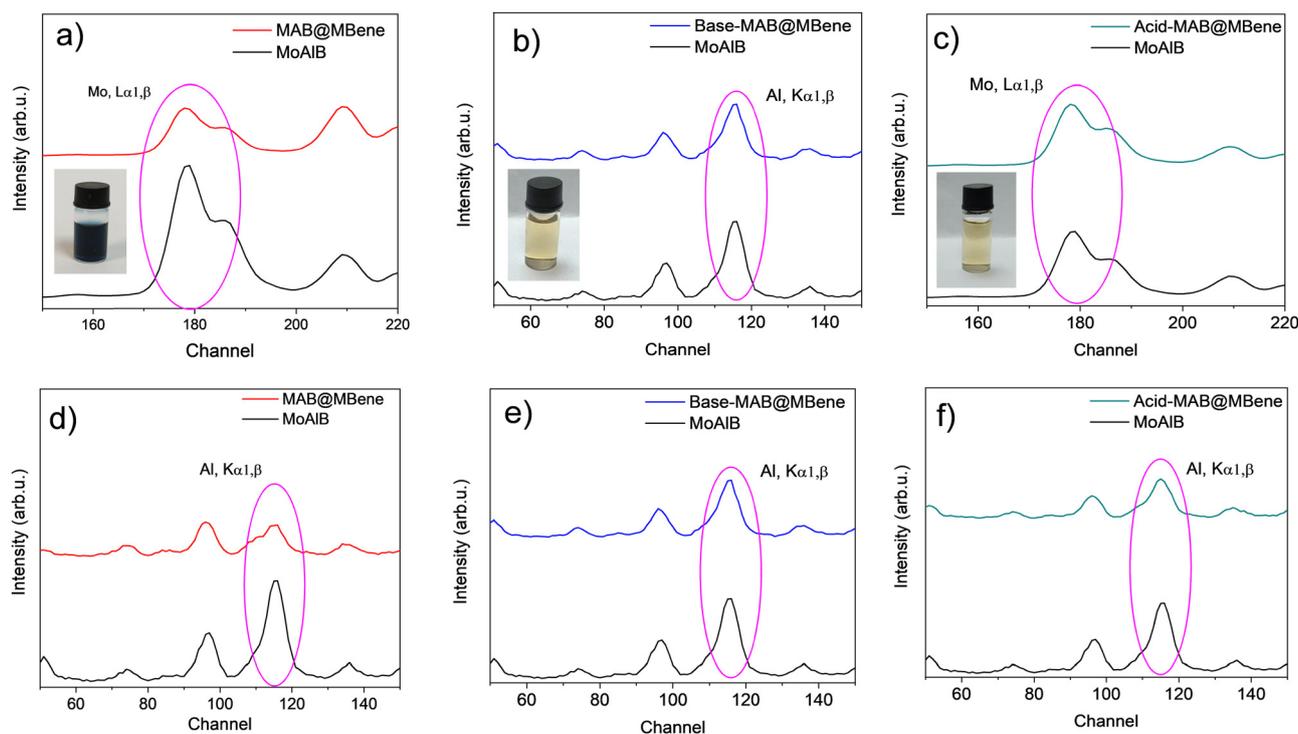Fig. 2 Analysis of the synthesis efficiency. XRF plots show Mo Lα peak for (a) MAB@MBene, (b) Base–MAB@MBene, (c) Acid–MAB@MBene as well as Al Kα peak for (d) MAB@MBene, (e) Base–MAB@MBene, and (f) Acid–MAB@MBene. The peak intensities were compared with the starting MoAlB. Insets (a–c) show digital photographs of the supernatant after the hydrothermal reaction.

hydrogen peroxide in combination with high temperature and pressure could partially oxidize the surface of molybdenum (Mo). These color changes preliminarily confirmed the effect of the pre-treatment on MAB etching. Therefore, we analyzed the obtained powders with XRF to reveal the amounts of Mo and Al in the samples, in contrast to the supernatant composition.

The XRF results of MAB@MBene, Acid-MAB@MBene, and Base-MAB@MBene are presented in Fig. 2. In the case of MAB@MBene, the Al peak decreased compared to the starting MoAlB, but so did the amount of Mo (Fig. 2a). The reason could be the leaching of Mo from the surface and the formation of MoO_2OH, resulting in a blue supernatant after the reaction.[21]

On the other hand, after pre-treatment, some edges might have opened and led to the etching of more Al, which is visible by the change in the Al content rather than the amount of Mo in Base-MAB@MBene (Fig. 2b) and Acid-MAB@MBene (Fig. 2c). The amount of Al was reduced the most in the Acid-MAB@MBene (Fig. 2f) as compared to the MAB@MBene (Fig. 2d) and Base-MAB@MBene (Fig. 2e). Also, the pretreated Acid-MAB@MBene supernatant has a higher intensity of Al. Therefore, from the XRF analysis, it can be concluded that the Acid-MAB@MBene's Al etching was better than the MAB@MBene and Base-MAB@MBene, although some amount of Al still remained.

We used scanning electron microscopy (SEM) and transmission electron microscopy (TEM) to analyze the outcome of our synthesis protocols. Microscopic images of the MoAlB starting phase are shown in Fig. 3a (SEM) and Fig. 3e (TEM). SEM and TEM images of the starting MoAlB phase showed its unetched and closely packed appearance. The MAB@MBene (Fig. 3b and f) exhibited a visible multilayered structure. This hybrid was not pre-treated before microwave-assisted hydrothermal etching. Hence, MoAlB should be directly introduced to the etching solution to achieve superficial etching. On the other hand, Base-MAB@MBene (Fig. 3c and g) and Acid-MAB@MBene (Fig. 3d and h) were deeply etched and formed an accordion-like structure, similar to MXene after etching from the MAX phase.[22,23]

SEM images confirm better etching than that achieved in previously reported works.[7,10,11] Almeda et al. showed that 10% NaOH treatment of MoAlB for 24 hours results in cavities of about 10 nm width and <100 nm depth, distributed periodically, and occurring once every 100–200 nm.[10] In the case of our Acid-MAB@MBene (Fig. 3d and h), the cavities range from nanometer to micrometer scale and can penetrate even to the core of the MoAlB grain. The insets added to Fig. 3a–d are the images of all diluted dispersions, which change from gray (MoAlB) to black (Acid-MAB@MBene). We assume this observation is another sign of suitable etching, as reported for MXene.[24]

When the Base-MAB@MBene was pre-treated with 0.1 M NaOH, the etching was improved and was not only limited to the surface. Furthermore, the Acid-MAB@MBene pre-treated with 0.1 M HCl showed much better results. In the case of the Acid-MAB@MBene, the etching reached the MAB core and created deep cavities (inset in Fig. 3h) along with the
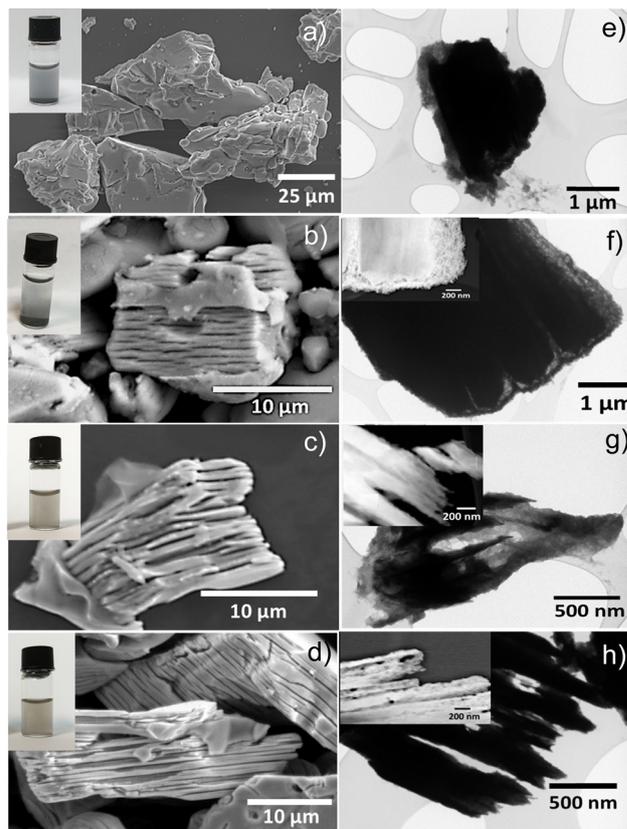

Fig. 3 SEM images of (a) MoAlB, (b) MAB@MBene, (c) Base-MAB@MBene, and (d) Acid-MAB@MBene. Insets show corresponding digital photographs of their diluted dispersions in water. TEM images of (e) MoAlB, (f) MAB@MBene, (g) Base-MAB@MBene, and (h) Acid-MAB@MBene added with insets showing their high-magnification images.

accordion-like structure of the final hybrid. It was more effective than previous reports in which etched regions were ~100 nm wide and separated from each other by <100 nm slabs.[7,10,11]

The claim of multilayered etching of the MoAlB phase is further supported by the HRTEM-EDS (high-resolution transmission electron microscopy-energy-dispersive X-ray spectroscopy) analysis shown in the ESI† (Fig. S3) and an elemental mapping (Fig. S4, ESI†) along with elemental composition with weight and atomic percentage in Tables S1–S4 in the ESI.† These results show a degree of etching change from MAB@MBene to Acid-MAB@MBene from its MoAlB phases. In TEM-EDS spectra, we also observed less Al content in Acid-MAB@MBene (Fig. S3c, ESI†) compared to MAB@MBene (Fig. S3a, ESI†) and Base-MAB@MBene (Fig. S3b, ESI†).

The same trend was observed in the EDS elemental analysis. In Fig. S4d (ESI†), Al K mapping shows the accordion-like structure (highlighted red circle), which is also visible in the SEM image (Fig. 3d). No similar structure is visible in the EDS mapping for the other hybrids, such as MoAlB (Fig. S4a, ESI†), MAB@MBene (Fig. S4b, ESI†), and Base-MAB@MBene (Fig. S4c, ESI†). Also, the elemental composition table of all four samples (MoAlB (Table S1, ESI†), MAB@MBene (Table S2, ESI†), Base-MAB@MBene (Table S3, ESI†) and Acid-MAB@MBene (Table S4, ESI†)) shows a gradual

reduction in Al content in terms of weight as well as the atomic percentage from MoAlB to Acid-MAB@MBene. The results obtained support our assumption on efficient etching of Al from MoAlB with protocols involving HCl pre-treatment before employing a microwave-assisted hydrothermal method.

We further recorded the X-ray diffraction (XRD, Fig. 4a) patterns to better understand the structure of the obtained hybrids. The XRD pattern of the MAB phase MoAlB matches well with previous reports (and PDF card no. 01-072-1277),[7,9] while changes are visible after the pre-treatments and etching. If complete etching of Al were achieved, (0k0) reflections would broaden and shift to lower angles, while other reflections (such as (110), (022), and (204)) would weaken significantly or disappear completely.[7] Here, most minor-intensity peaks (such as (110), (021), (022) and (204)) of MoAlB decreased in MAB@MBene and completely disappeared in Acid-MAB@MBene. This indicates that the Al content decreased compared to the MoAlB observed in the EDS and elemental analysis.

Simultaneously, the intensity of the (0k0) peaks (such as (020), (040), (060)) increased ~3 times in Acid-MAB@MBene. Increasing intensity indicates a higher degree of order, arrangement, and crystalline phase. This implies that Acid-MAB@MBene converts into a single phase from bulk (unetched) but is still in the MoAlB phase, as observed in Fig. 3h. Therefore, pre-treatment with 0.1 M NaOH and HCl and the microwave-assisted hydrothermal method appear to be effective for obtaining mono-phase MAB etched on the surface.

The surface charge should be further considered if the surface is being analyzed. The zeta potential is a sensitive parameter that tracks any changes in the chemical composition of the surface. Fig. 4b shows the zeta potential measured for all three hybrids and compared to the starting MoAlB. It changes from −10 mV for unetched MoAlB to −19 mV for MAB@MBene, −15 mV for Base-MAB@MBene, and −11 mV for Acid-MAB@MBene.

This observation agrees with etched and delaminated MXenes, which achieved a zeta potential of over −20 mV for well-etched samples.[25] This negative zeta potential indicates that the surface is negatively charged, enabling it to attract positively charged surfaces. This property can be utilized in photocatalysis, sensors, and surface coatings. Similar activities have been observed in various MXenes or MBenes.[13,26–28]

The X-ray photoelectron spectroscopy (XPS) analysis was performed in the next step to reveal the chemical composition of the etched MBenes' surface. The quantitative XPS data for MAB@MBene (Fig. 5a), Base-MAB@MBene (Fig. 5b), and Acid-MAB@MBene (Fig. 5c) are provided in ESI,† Tables S5, S6 and S7, respectively. The analysis considers the deconvolution of the molybdenum (Mo 3d), aluminum (Al 2p), and boron (B 1s) signals, viz., the key elements of the samples.

The high-resolution XPS Mo 3d signal for MAB@MBene (Fig. 5a) is fitted into two oxide components with different oxidation states, i.e., Mo(v) and Mo(vi). The peak position of both Mo(v & vi) oxides is in good agreement with previous studies conducted by Spevak et al.[29] and Baltrusaiti et al.[30] However, we did not observe the presence of molybdenum boride at the surface. The boride XPS peak should be located at 227.8 ± 0.5 eV.[31] Thus, the value of boride is far from the current Mo 3d peak in this study, i.e., 231.3 eV (3.5 eV difference). It is important to highlight the calibration error of C 1s, which usually occurs in the range of ±0.5 eV.[32] Therefore, we can neglect the factor of calibration error.

The Al 2p spectrum shows a single peak that can be assigned to Al_2O_3, which may come from MoAlB etching.[31,33] Fig. 5a shows the XPS spectra of B 1s, located at 192.8 eV. This peak can be assigned to a common B_2O_3 component, but the value slightly deviates from the current result, i.e., 188.1 (4.7 eV).[31,33] We cannot see any boride-related spectra from B 1s and Mo 3d. Thus, we can strongly conclude that no boride is present on the surface of MAB@MBene.

For Base-MAB@MBene (Fig. 5b), we can see the contribution of $MoCl_5$ in the Mo 3d spectra.[29] The XPS spectra of Al 2p shows a contribution from three deconvoluted peaks, i.e. Al_2O_3, AlOH or AlO(OH), and $AlCl_3$.[31,33] Interestingly, the contribution of AlO(OH) is dominant compared to the oxide. This trend is slightly different from the one we found in the MAB@MBene.
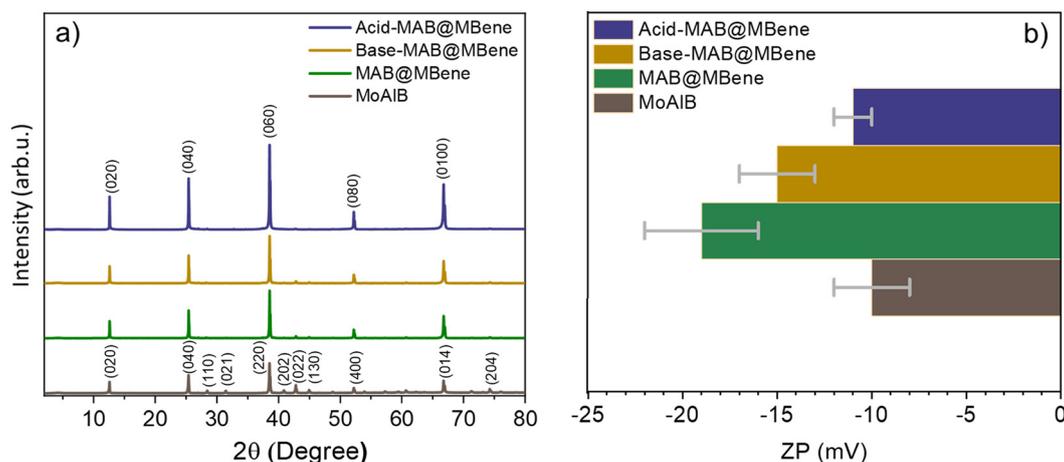

Fig. 4 (a) XRD diffraction patterns and (b) zeta potential of MoAlB, MAB@MBene, Base-MAB@MBene and Acid-MAB@MBene.
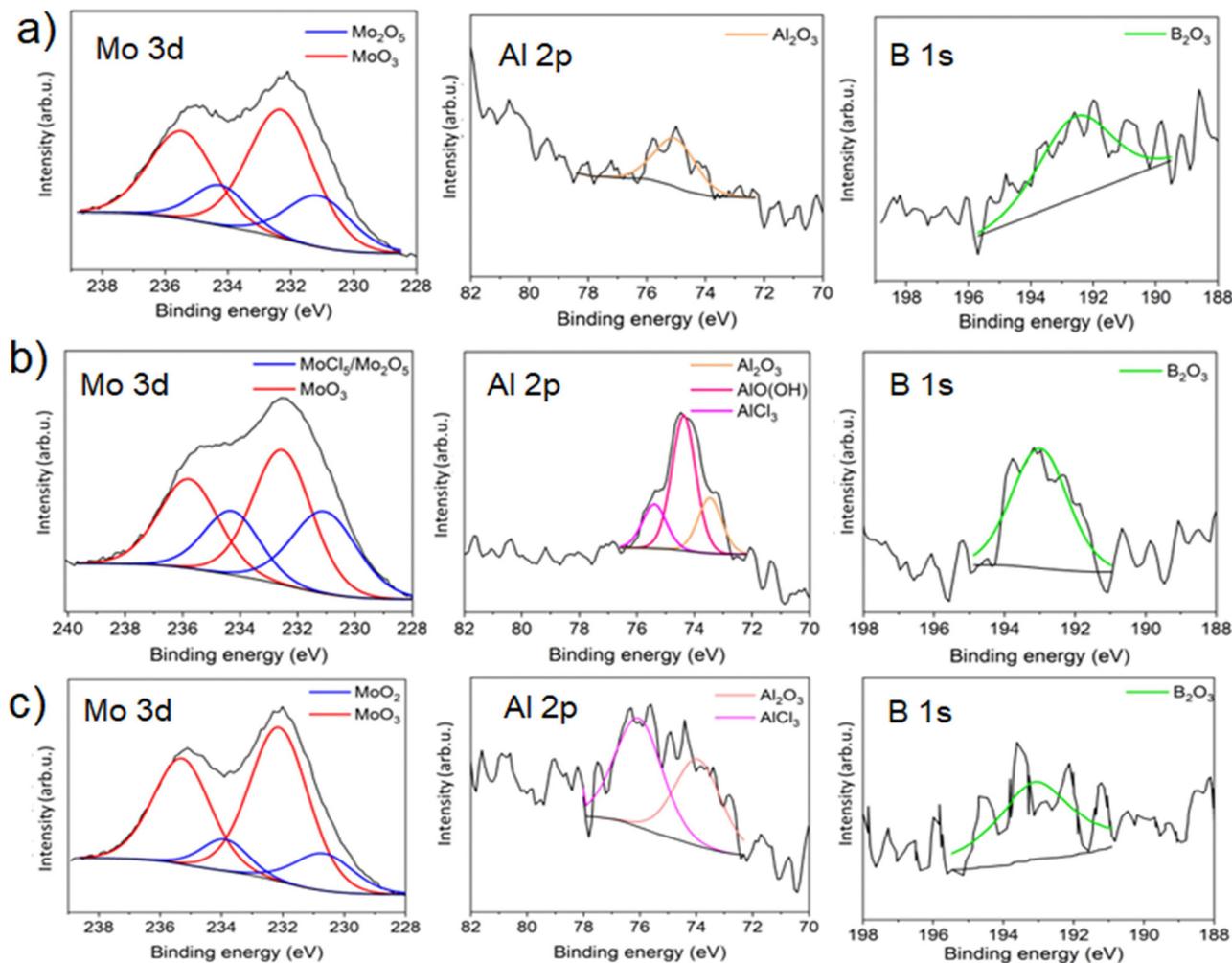
Fig. 5 X-ray photoelectron spectroscopy (XPS) peak deconvolution of Mo 3d, Al 2p, and B 1s of (a) MAB@MBene, (b) Base-MAB@MBene and (c) Acid-MAB@MBene.

Its B 1s spectrum was shifted a little to a higher energy compared to the MAB@MBene. Thus, there may be a contribution from multispecies, *i.e.*, B_2O_3 (H_3BO_3). Again, no trace of the boride component from the XPS spectra of B 1s can be observed.

For the Acid-MAB@MBene (Fig. 5c) sample, the XPS spectrum of Mo 3d is different from MAB@MBene and Base-MAB@MBene. Here, the difference between the Mo components of all three batches comes from the different synthesis protocols. The presence of MoO_3 aligns well with the yellow-colored supernatant (inset in Fig. 2c). The Al 2p XPS spectra of this sample come from the contribution of Al_2O_3 and $AlCl_3$. Furthermore, we cannot detect the boride peak but rather the oxide (B_2O_3) peak.

Note that XPS analysis is a surface measurement technique, reaching up to 500 nm into the sample.[34,35]

Therefore, we mainly obtained surface results after etching the MoAlB, which is reasonable. We conclude that the MAB grains are covered with a layer composed of different species,

such as Al_2O_3, $AlCl_3$, MoO_3, $MoCl_5$, and B_2O_3, due to the oxidation of the surface. Few reports confirm the formation of such species while etching and processing MAB phases.[34,35] We also did not find an $AlCl_3$ peak in MAB@MBene, which is present in Base-MAB@MBene and Acid-MAB@MBene. The presence of $AlCl_3$ could result in a yellow supernatant after hydrothermal treatment, as $AlCl_3$ also shows a pale yellow color.[20]

We also performed Fourier-transform infrared (FTIR) spectroscopy measurements (Fig. S5, ESI†) to learn more about our hybrids' surface functionalization and the eventual presence of covalent bonding. Boron-based covalent bonds were observed after etching compared to their lack of MoAlB. The band near ~1100 cm^{-1} corresponds well to B–OH functional groups, which are observed in the 1000–1300 cm^{-1} peak range.[36,37]

The peak around 1300–1350 cm^{-1} is characteristic of B–O stretching vibrations, which occurs due to the presence of the oxy-functional groups of boron.[37–39] This observation solves the issue of why the XPS results show the presence of B_2O_3 on the

surface. The peak at ~1600 cm^{-1} can be assigned to B–H as a B–H–B bridge. The hydroxyl group B–OH was observed near 3000 cm^{-1}, which could be attributed to absorbed moisture.[36,37,39,40]

Therefore, the etched MoAlB should have hydroxyl, hydride, and oxy-functional groups on the surface, supporting our XPS findings. The newly developed microwave-assisted method with pre-treatment is a mild route for etching MAB into the multi-layered MAB@MBene phase in less time than conventional wet chemical etching.

3.3. Optical properties

After understanding the chemical composition of our samples, we moved on to optical studies. The presence of superficial oxides could enable the interesting optical activity of our multi-layered MBene structures. We first recorded the optical absorbance of these materials in water dispersions (Fig. 6a) and in the form of dried powder (Fig. 6b). The liquid dispersion of MAB@MBene showed a small curve (highlighted by a green rectangle). While Acid-MAB@MBene and Base-MAB@MBene exhibited no absorption peak in the 400–1000 nm range, which indicates a metallic behavior for its aqueous dispersion. Helmar *et al.* also observed a similar trend for a Mo$_{4/3}$B$_{2-x}$T$_z$ aqueous dispersion.[41] Powder samples showed a small, broad peak around 500–800 nm due to the metal oxide shell on the MAB surface, as confirmed from the XPS analysis.[42]

Moving on to the absorption in the deep UV region, we observed a clear absorption edge of MoAlB, MAB@MBene, Base-MAB@MBene, and Acid-MAB@MBene (Fig. 6c and d), which we attributed to the band-to-band transition of the metal oxide on the surface of the etched MoAlB (most likely Mo-based

oxides). Moreover, the estimated bandgap of the samples based on the absorption spectra are 3.54, 3.58, 3.65, and 3.88 eV, for MoAlB, MAB@MBene, Acid-MAB@MBene, and Base-MAB@MBene (Fig. S6a–d, ESI†), respectively. A possible reason for the band gap variation is an effect of the different etching approaches, functionalization of etched MoAlB, and formation of metal oxide (MoO$_2$, MoO$_3$, or Mo$_2$O$_5$) on its surface.[41] In MXene, such factors also play an important role in tuning the optical properties, which are well-proven theoretically and experimentally.[43,44]

The Ψ and Δ at the incident angle of 45° of the representative sample (MAB@MBene) are shown in Fig. S1 (ESI†). The optical model fits the experimental data well. After the fitting process, the optical constants of the sample, *i.e.*, refractive index (n) and extinction coefficients (k), were obtained. The results for Δn and Δk are presented by calculating the differences to MoAlB (the MAB phase). This approach provides a comparative insight into the variation across MAB@MBene with different synthesis treatments.

Acid-MAB@MBene showed the smallest difference of Δn compared to MAB@MBene and Base-MAB@MBene (Fig. 6e). Fig. S7a (ESI†) shows the n value of the samples at a wavelength of 300–800 nm (1.55–4.13 eV). In this context, Base-MAB@MBene showed the highest n value (~1.37) over the measured spectral range, implying the highest capability to refract electromagnetic waves. Furthermore, the other MBene samples, *i.e.*, Acid-MAB@MBene and MAB@MBene, showed n values of ~1.17 and ~1.36, respectively.

Here, all three etched samples showed higher n values than the MoAlB, whose n value was ~1.08, implying the hydrothermal treatment could modify the optical properties.[45] However, the
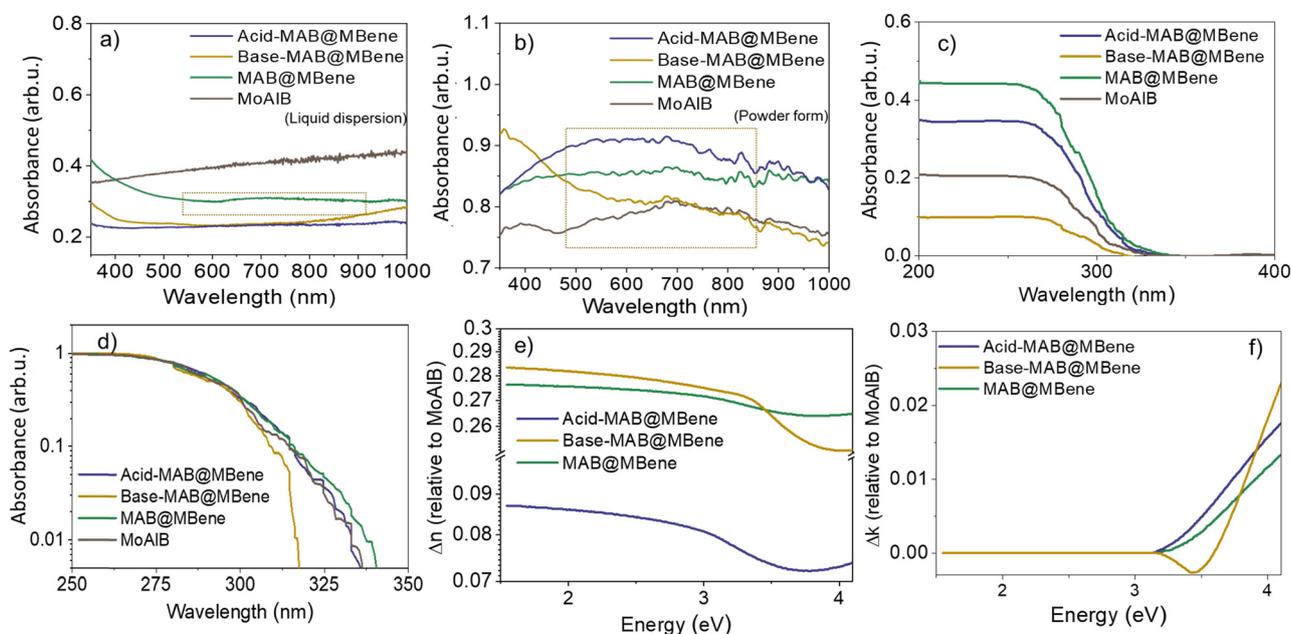

Fig. 6 Optical absorption analysis (a) UV-vis spectra in liquid dispersions (b) solid-state UV-vis absorption spectra. The rectangles in (a) and (b) highlight the peak. (c) and (d) the deep UV region absorption spectra of MoAlB, MAB@MBene, Base-MAB@MBene, and Acid-MAB@MBene. The (e) relative refractive index (Δn) and (f) extinction coefficient (Δk) of MAB@MBene, Base-MAB@MBene, and Acid-MAB@MBene in comparison to MoAlB.

value obtained in this experiment differs from the n value of MoAlB obtained theoretically (3–7 at an energy range of 0–5 eV).[17,46] This may indicate that our materials are not MoAlB phase alone but have a MoAlB@MBene multilayered structure.

The Δk value of all the samples shows a similar trend for the energy below 3.14 eV (Fig. 6f). However, the MAB@MBene, Base-MAB@MBene, and Acid-MAB@MBene displayed different intensity levels and blue shifting in the UV region. This shifting can be connected to a shift in the bandgap value of the sample, which is shown in Fig. S6 (ESI†).[47,48] Notably, Base-MAB@MBene showed the most significant shift in the absorption edge toward higher energy. To be specific, the k spectra of all the samples only show a single maximum of ~ 300 nm, which is attributed to the oxide phase on the surface of the etched MoAlB.

Next, we explore the charge carrier dynamics of the MBene samples *via* steady-state and time-resolved photoluminescence (TRPL) analysis. MAB@MBene, Base-MAB@MBene, and Acid-MAB@MBene showed a bandgap value in the UV region, which was observed in the absorbance spectra (Fig. 6c and d). Consequently, we performed photoluminescence measurements with high excitation energy (266 nm). All three samples exhibited identical peaks in the visible region centered at 682 and 516 nm (Fig. S8a, ESI†).

The most plausible origin of these peaks is the recombination of electrons to defects in the interfacial oxide of the MBene. Furthermore, we monitored the emission above 600 nm by TRPL to study the charge carrier dynamics. MAB@MBene, Base-MAB@MBene, and Acid-MAB@MBene (Fig. S8b–d, ESI†) showed tri-exponential decay with an average carrier lifetime of 2.0, 2.1, and 1.9 μs, respectively, which is also tabulated in Table S8 (ESI†) with another parameter. This large decay time may indicate the trapping and de-trapping process of electrons due to the presence of defects.[49,50] Since defects can alter the density of traps, they often act as non-radiative recombination centers.[48,51] To sum up, the UV absorption characteristic and tunable refractive index of MBene promise that it can be applied as UV photodetectors, lasers, and UV shielding for space applications.

Although analyzing the optical properties of ML MoAlB@MBene faces challenges due to multilayer formation, surface oxide, and defects, these aspects can be beneficial depending on the application. Trace amounts of aluminum may also affect optical properties, but this can be resolved by further delamination to form single layers, similar to MXene.

4. Plausible reaction mechanism of etching

To elucidate the reaction mechanism of Al etching from the MoAlB MAB phase, we present a schematic representation of the etching process at each stage and the possible material conditions (Fig. 7). SEM and TEM micrographs have been used to illustrate the etching process and its effects on the material. The previous section has already discussed pretreatment possible reactions, with reactions (1) and (2) supported by the XRF results (Fig. S2, ESI†).

In the second step of the microwave-assisted hydrothermal method, a combination of 0.6 M HCl and H_2O_2 (30%) has been chosen to facilitate possible reactions (3)–(10). Based on the introductory reaction chemistry, the following plausible
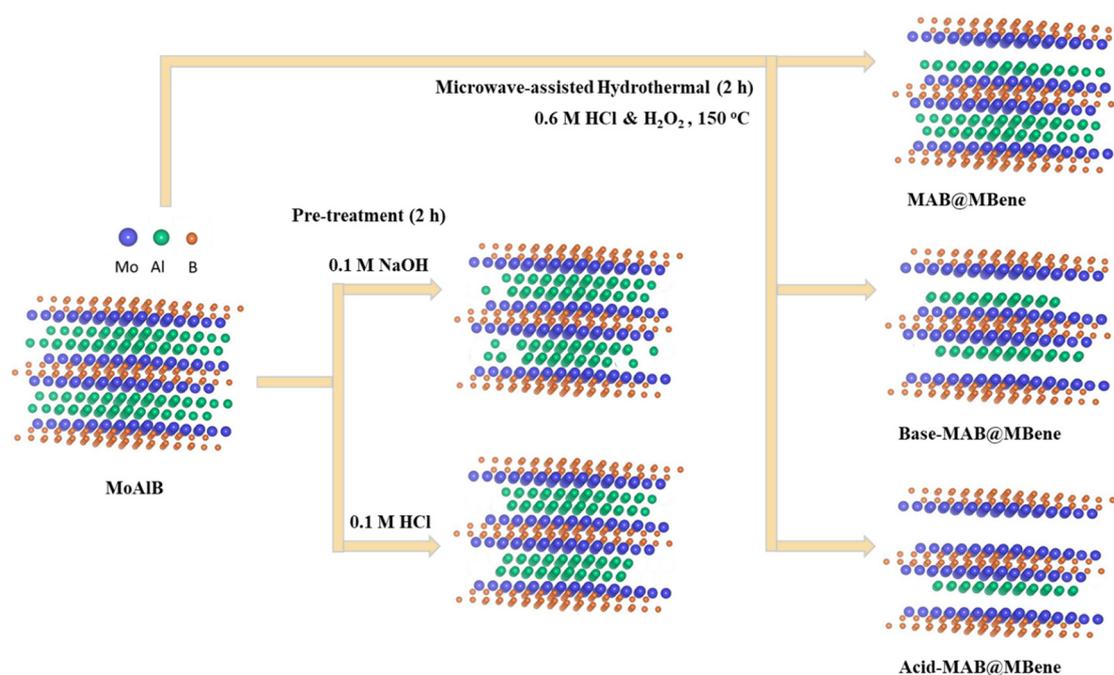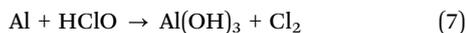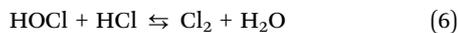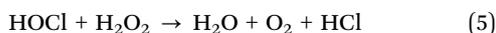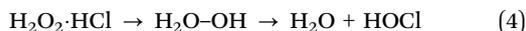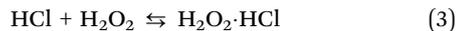

Fig. 7 Schematic illustration of different stages of aluminum (Al) etching from the MoAlB MAB phase for multilayer (ML) MoAlB@MBene *via* pretreatment and microwave-assisted hydrothermal method.
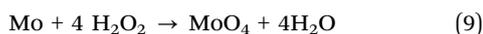
reactions are presented for the microwave-assisted hydrothermal method.[20,52,53]

$$HCl + H_2O_2 \leftrightarrows H_2O_2 \cdot HCl \quad (3)$$

$$H_2O_2 \cdot HCl \rightarrow H_2O-OH \rightarrow H_2O + HOCl \quad (4)$$

$$HOCl + H_2O_2 \rightarrow H_2O + O_2 + HCl \quad (5)$$

$$HOCl + HCl \leftrightarrows Cl_2 + H_2O \quad (6)$$

$$Al + HClO \rightarrow Al(OH)_3 + Cl_2 \quad (7)$$

H_2O_2 is one of the most powerful oxidizing agents. When dissolved in water, hydrogen peroxide acts as a weak acid. Maass and Hiebert demonstrated the reaction rate and performance between H_2O_2 and HCl.[52,53] This reaction forms a complex, $H_2O_2 \cdot HCl$ (reaction (3)), which further breaks down into hypochlorous acid and water (reaction (4)). Subsequently, hypochlorous acid reacts with hydrogen peroxide, releasing chlorine (reactions (5) and (6)).[52,53] Additionally, hypochlorous acid can react with Al from MoAlB, forming $Al(OH)_3$ and resulting in etching (reaction (7)).[20,54,55]

It is unlikely that such a reaction can occur with Mo (molybdenum) because Mo is known to easily form a thin layer of oxide on its surface, which protects it from further reaction and corrosion.[20,56,57] Therefore, the process remains very slow as long as the MoO_2 passivation layer remains nearly intact. While some reactions do occur with Mo, the formation of oxide and chloride (reaction (8)–(10))[20,56,57] has been observed and confirmed through XPS results. The color of the supernatant after the microwave-assisted hydrothermal reaction is due to Mo-based species. In the case of MAB@MBene supernatant, the blue color indicates a mild reduction of the aqueous or acidic solution of molybdates (MoO_3) with the (+IV/V) oxidation state (reaction (9)).[20,56,57] Conversely, the yellow color supernatant for Base-MAB@MBene and Acid-MAB@MBene could result from either the formation of hydrated oxides ($MoO_3 \cdot 2H_2O$) or molybdenum oxychloride (MoO_2Cl_2), both of which are yellow in color.[20,56,57]

$$Mo + 3HCl + 3Cl^- \rightarrow MoCl_6^{3-} + 3/2H_2 \quad (8)$$

$$Mo + 4 H_2O_2 \rightarrow MoO_4 + 4H_2O \quad (9)$$

$$2Mo + 3O_2 \rightarrow 2MoO_3 \quad (10)$$

In the case of molybdenum (Mo), predicting the reaction pathway is more challenging due to the formation of various complexes in the solution. A key characteristic of Mo's chemistry is the formation of polyacids. The polyacids of Mo are not fully understood because the degree of hydration and protonation of the various species in the solution is unknown.[20,56,57]

The different order of Al etching ultimately depends on the pretreatment. We have already observed more Al content in the 0.1 M HCl step than in 0.1 M NaOH (Fig. S2, ESI†). Therefore, in the case of Acid-MAB@MBene, this initiation of etching and opening up more surfaces for better Al etching led to a better multilayer structure till its core. This plausible reaction mechanism is predicted and supported through XRF, XPS, EDS results, and SEM and TEM micrographs. A detailed analysis of reaction kinetics and

mechanism has been reported for etching MAX to MXene.[55,58] However, an in-depth understanding and presentation of the reaction mechanism from MoAlB to MBene using various techniques are still needed. This would provide a new platform for researchers.

5. Conclusions

Herein, our study explored the impact of acid (HCl) and base (NaOH) treatments combined with a mild microwave-assisted hydrothermal approach on Al etching from the MoAlB MAB phase. We successfully developed an easy, efficient, straightforward etching technique that surpasses previous methods. Unlike traditional selective etching requiring prolonged durations and highly concentrated chemicals, our method minimizes incomplete etching, complete oxidation, and corrosion of MAB phases. We achieved effective Al etching from MoAlB using the microwave-assisted hydrothermal method in just 4 hours by incorporating HCl or NaOH pre-treatments.

Our findings reveal that the resulting multilayered MoAlB@MBene structures exhibit unique and tailored optical properties. SEM and TEM images demonstrate Al etching from the edges, forming a MXene-like accordion structure. XRF, XRD, and SEM-EDS analyses confirm the initiation of Al etching through pre-treatment, reducing Al content and forming a multilayer (ML) MBene structure. The optical band gap of MoAlB@MBene ranges from 3.54 to 3.88 eV, indicating its potential for various light-based applications. The etched MoAlB@MBene structures also display higher refractive index (n) values and varying intensity levels with blue shifting in the UV region for the excitation coefficient (k).

Our results validate the effectiveness of the microwave-assisted hydrothermal method, highlighting its potential to etch Al from the MAB phase efficiently. This method offers advantages such as reduced use of harsh chemicals, shorter synthesis duration, and improved material homogeneity. Aluminum can be etched within a day, producing high-quality and uniform structures. However, further studies are needed to understand the effects of multi- and single-layer MBenes on optical properties and stability after acid/base etching and delamination for potential optoelectronic applications.

In conclusion, our work demonstrates the ability to tune the optical properties of ML MoAlB@MBene through different etching techniques. The limited availability of MBene-like borides will allow us to explore the role of boron in their properties. Our analysis suggests that boron-containing multilayered MBenes with surface oxides could outperform other 2D materials, including graphene and MXene. Consequently, further research on MBenes should focus on developing efficient etching and delamination methods and exploring their applications in optoelectronic devices.

Author contributions

MC designed the concept and content of the experiment, prepared and characterized the MBene samples, collected and

analyzed the obtained results, designed the figures, prepared the original manuscript draft, MAKP performed the XPS data and optical analysis, DK performed the optical measurements, LT performed the PL and time-resolved PL, DM carried out the XRD measurements, AW carried out the HRTEM measurements, MDB analyzed the optical measurements and corrected the original manuscript, MN synthesized the MAB phase (MoAlB) and corrected the original manuscript, AJ acquired the funding, coordinated and supervised the preparation of the manuscript, coordinated the research, and corrected the original manuscript. The manuscript was written through the contributions of all authors. All authors have approved the final version of the manuscript.

Data availability

The data supporting this article have been included in the ESI.† Also, the data that support the findings of this manuscript are available upon request from the corresponding author.

Conflicts of interest

There are no conflicts to declare.

Acknowledgements

References

1 V. G. Nair, M. Birowska, D. Bury, M. Jakubczak, A. Rosenkranz and A. M. Jastrzębska, *Adv. Mater.*, 2022, **34**, 2108840.

2 A. Rosenkranz, D. Zambrano, A. Przyborowski, R. Shah and A. M. Jastrzębska, *Adv. Mater. Interfaces*, 2022, **9**, 2200869.

3 A. Hayat, T. Bashir, A. M. Ahmed, Z. Ajmal, M. M. Alghamdi, A. A. El-Zahhar, M. Sohail, M. A. Amin, Y. Al-Hadeethi, E. Ghasali, S. Raza and Y. Orooji, *Mater. Sci. Eng.: R: Rep.*, 2024, **159**, 100796.

4 M. Ade and H. Hillebrecht, *Inorg. Chem.*, 2015, **54**, 6122–6135.

5 M. Khazaei, J. Wang, M. Estili, A. Ranjbar, S. Suehara, M. Arai, K. Esfarjani and S. Yunoki, *Nanoscale*, 2019, **11**, 11305–11314.

6 W. Jeitschko, *Monatsh. Chem.*, 1966, **97**, 1472–1476.

7 L. T. Alameda, C. F. Holder, J. L. Fenton and R. E. Schaak, *Chem. Mater.*, 2017, **29**, 8953–8957.

8 J. Zhou, J. Palisaitis, J. Halim, M. Dahlqvist, Q. Tao, I. Persson, L. Hultman, P. O. Å. Persson and J. Rosen, *Science*, 2021, **373**, 801–805.

9 A. Majed, M. Torkamanzadeh, C. F. Nwaokorie, K. Eisawi, C. Dun, A. Buck, J. J. Urban, M. M. Montemore, V. Presser and M. Naguib, *Small Methods*, 2023, **7**, 2300193.

10 L. T. Alameda, P. Moradifar, Z. P. Metzger, N. Alem and R. E. Schaak, *J. Am. Chem. Soc.*, 2018, **140**, 8833–8840.

11 L. T. Alameda, R. W. Lord, J. A. Barr, P. Moradifar, Z. P. Metzger, B. C. Steimle, C. F. Holder, N. Alem, S. B. Sinnott and R. E. Schaak, *J. Am. Chem. Soc.*, 2019, **141**, 10852–10861.

12 S. Kota, E. Zapata-Solvas, A. Ly, J. Lu, O. Elkassabany, A. Huon, W. E. Lee, L. Hultman, S. J. May and M. W. Barsoum, *Sci. Rep.*, 2016, **6**, 26475.

13 D. Bury, M. Jakubczak, M. A. K. Purbayanto, M. Rybak, M. Birowska, A. Wójcik, D. Moszczyńska, K. Eisawi, K. Prenger, V. Presser, M. Naguib and A. M. Jastrzębska, *Adv. Funct. Mater.*, 2023, **33**, 2308156.

14 J. Guo, Y. Hao, A. V. Kuklin, W. Bao, S. Wageh, O. A. Al-Hartomy, A. G. Al-sehemi, H. Ågren, L. Gao and H. Zhang, *ACS Photonics*, 2023, **10**, 2353–2362.

15 Y. Wang, G. Wang, Y. Wang, L. Zhou, J. Kang, W. Zheng, S. Xiao, G. Xing and J. He, *J. Phys. Chem. Lett.*, 2024, **15**, 3461–3469.

16 M. Jakubczak, A. Wojciechowska, D. F. Zambrano, D. Moncada, M. Birowska, D. Moszczyńska, K. Eisawi, M. Naguib, A. Rosenkranz and A. M. Jastrzębska, *Appl. Mater. Today*, 2023, **35**, 101925.

17 X. Li, H. Cui and R. Zhang, *Sci. Rep.*, 2016, **6**, 39790.

18 L.-Y. Meng, B. Wang, M.-G. Ma and K.-L. Lin, *Mater. Today Chem.*, 2016, **1–2**, 63–83.

19 N. Abid, A. M. Khan, S. Shujait, K. Chaudhary, M. Ikram, M. Imran, J. Haider, M. Khan, Q. Khan and M. Maqbool, *Adv. Colloid Interface Sci.*, 2022, **300**, 102597.

20 J. D. Lee, *Concise Inorganic Chemistry*, Blackwell Science, 1998.

21 E. R. Braithwaite and J. Haber, *Molybdenum: An Outline of its Chemistry and Uses*, Elsevier, 2013.

22 K. R. G. Lim, M. Shekhirev, B. C. Wyatt, B. Anasori, Y. Gogotsi and Z. W. Seh, *Nat. Synth.*, 2022, **1**, 601–614.

23 M. Naguib, M. Kurtoglu, V. Presser, J. Lu, J. Niu, M. Heon, L. Hultman, Y. Gogotsi and M. W. Barsoum, *Adv. Mater.*, 2011, **23**, 4248–4253.

24 K. Maleski, C. E. Shuck, A. T. Fafarman and Y. Gogotsi, *Adv. Opt. Mater.*, 2021, **9**, 2001563.

25 A. Rozmysłowska-Wojciechowska, A. Szuplewska, T. Wojciechowski, S. Poźniak, J. Mitrzak, M. Chudy, W. Ziemkowska, L. Chlubny, A. Olszyna and A. M. Jastrzębska, *Mater. Sci. Eng., C*, 2020, **111**, 110790.

26 S. K. Azadi, M. Zeynali, S. Asgharizadeh and M. A. Fooladloo, *Mater. Today Commun.*, 2023, **35**, 106136.

27 L. Dong, H. Chu, Y. Li, X. Ma, H. Pan, S. Zhao and D. Li, *Appl. Mater. Today*, 2022, **26**, 101341.

28 G. R. Berdiyorov, *AIP Adv.*, 2016, **6**, 055105.

29 P. A. Spevack and N. S. McIntyre, *J. Phys. Chem.*, 1992, **96**, 9029–9035.

30 J. Baltrusaitis, B. Mendoza-Sanchez, V. Fernandez, R. Veenstra, N. Dukstiene, A. Roberts and N. Fairley, *Appl. Surf. Sci.*, 2015, **326**, 151–161.

31 J. R. Rumble Jr., D. M. Bickham and C. J. Powell, *Surf. Interface Anal.*, 1992, **19**, 241–246.

32 J. Halim, K. M. Cook, M. Naguib, P. Eklund, Y. Gogotsi, J. Rosen and M. W. Barsoum, *Appl. Surf. Sci.*, 2016, **362**, 406–417.

33 J. F. Moulder, *Handbook of X-ray Photoelectron Spectroscopy: A Reference Book of Standard Spectra for Identification and Interpretation of XPS Data*, Physical Electronics Division, PerkinElmer Corporation, 1992.

34 N. Gauthier, C. Courrèges, J. Demeaux, C. Tessier and H. Martinez, *Appl. Surf. Sci.*, 2020, **501**, 144266.

35 T. S. Nunney, O. Mustonen, P. Mack, J. Wolstenholme and B. R. Strohmeier, in *2011 37th IEEE Photovoltaic Specialists Conference*, 2011, p. 001333.

36 G. Socrates, *Infrared and Raman Characteristic Group Frequencies: Tables and Charts*, John Wiley & Sons, 2004.

37 A. L. James and K. Jasuja, *RSC Adv.*, 2017, **7**, 1905–1914.

38 S. Gupta, I. Z. Hlova, T. Kobayashi, R. V. Denys, F. Chen, I. Y. Zavaliy, M. Pruski and V. K. Pecharsky, *Chem. Commun.*, 2013, **49**, 828–830.

39 D. K. Aswal, K. P. Muthe, A. Singh, S. Sen, K. Shah, L. C. Gupta, S. K. Gupta and V. C. Sahni, *Phys. C*, 2001, **363**, 208–214.

40 W. G. Shin, S. Calder, O. Ugurlu and S. L. Girshick, *J. Nanopart. Res.*, 2011, **13**, 7187–7191.

41 P. Helmer, J. Halim, J. Zhou, R. Mohan, B. Wickman, J. Björk and J. Rosen, *Adv. Funct. Mater.*, 2022, **32**, 2109060.

42 E. Pavoni, M. G. Modreanu, E. Mohebbi, D. Mencarelli, P. Stipa, E. Laudadio and L. Pierantoni, *Nanomaterials*, 2023, **13**(8), 1319.

43 K. Chaudhuri, Z. Wang, M. Alhabeb, K. Maleski, Y. Gogotsi, V. Shalaev and A. Boltasseva, in *2D Metal Carbides and Nitrides (MXenes): Structure, Properties and Applications*, ed. B. Anasori and Y. Gogotsi, Springer International Publishing, Cham, 2019, pp. 327–346.

44 B. Fu, J. Sun, C. Wang, C. Shang, L. Xu, J. Li and H. Zhang, *Small*, 2021, **17**, 2006054.

45 F. Majid, M. Bashir, I. Bibi, A. Raza, S. Ezzine, N. Alwadai and M. Iqbal, *J. Mater. Res. Technol.*, 2022, **18**, 4019–4029.

46 B. O. Mnisi, *Mater. Res. Express*, 2021, **8**, 096533.

47 M. A. Kenichi Purbayanto, A. Rusydi and Y. Darma, *Phys. Chem. Chem. Phys.*, 2020, **22**, 2010–2018.

48 M. A. K. Purbayanto, E. Nurfani, M. A. Naradipa, R. Widita, A. Rusydi and Y. Darma, *Opt. Mater.*, 2020, **108**, 110418.

49 M. A. K. Purbayanto, E. Nurfani, O. Chichvarina, J. Ding, A. Rusydi and Y. Darma, *Appl. Surf. Sci.*, 2018, **462**, 466–470.

50 A. Redinger, S. Levcenko, C. J. Hages, D. Greiner, C. A. Kaufmann and T. Unold, *Appl. Phys. Lett.*, 2017, **110**, 122104.

51 M. Wang, B. Li, J. Yuan, F. Huang, G. Cao and J. Tian, *ACS Appl. Mater. Interfaces*, 2018, **10**, 37005–37013.

52 O. Maass and P. G. Hiebert, *J. Am. Chem. Soc.*, 1924, **46**, 290–308.

53 R. S. Livingston and W. C. Bray, *J. Am. Chem. Soc.*, 1925, **47**, 2069–2082.

54 X.-H. Guo, Y. Yang and Z.-Y. Deng, *ACS Omega*, 2021, **6**, 14182–14190.

55 Y.-J. Kim, S. J. Kim, D. Seo, Y. Chae, M. Anayee, Y. Lee, Y. Gogotsi, C. W. Ahn and H.-T. Jung, *Chem. Mater.*, 2021, **33**, 6346–6355.

56 M. Motasim, T. Agacayak, Y. R. Eker, S. Aydogan and A. Abbaker, *Can. J. Chem. Eng.*, 2024, **1**, DOI: **10.1002/cjce.25530**.

57 V. A. Volkovicha, T. R. Griffiths, R. C. Thied and B. Lewin, *J. Nucl. Mater.*, 2003, **323**, 93–100.

58 M. Anayee, C. E. Shuck, M. Shekhirev, A. Goad, R. Wang and Y. Gogotsi, *Chem. Mater.*, 2022, **34**, 9589–9600.